Dimensions of a Projection Column and Architecture of VPM and POm Axons in Rat Vibrissal Cortex

Verena C. Wimmer[1,2], Randy M. Bruno[1,3], Christiaan P.J. de Kock[1,4], Thomas Kuner[1,5] and Bert Sakmann[1,6,7,8]

[1]Department of Cell Physiology, Max Planck Institute for Medical Research, D-69120 Heidelberg, Germany

[2]Current address: Florey Neuroscience Institutes, The University of Melbourne, Parkville 3010, Victoria, Australia
[3]Current address: Department of Neuroscience, Columbia University, New York, NY 10027, USA
[4]Current address: Center for Neurogenomics and Cognitive Research, Neuroscience Campus Amsterdam, VU University Amsterdam, NL-1087 HV Amsterdam, the Netherlands
[5]Current address: Institute for Anatomy and Cell Biology, University of Heidelberg, 69120 Germany
[6]Current address: Max Planck Florida Institute, Jupiter, FL 33458, USA
[7]Current address: Research Group Cortical Column in Silico, Max Planck Institute for Neurobiology, D-82152 Martinsried, Germany
[8]Current address: Department of Digital Neuroanatomy, Max Planck Florida Institute for Integrative Biology and neuroscience, Jupiter, FL 33458, USA

Address correspondence to Verena C. Wimmer, Florey Neuroscience Institutes, Parkville 3010, Victoria, Australia. Email: Verena.Wimmer@florey.edu.au.

This is the first article in a series of 3 studies that investigate the anatomical determinants of thalamocortical (TC) input to excitatory neurons in a cortical column of rat primary somatosensory cortex (S1). S1 receives 2 major types of TC inputs, lemiscal and paralemniscal. Lemiscal axons arise from the ventral posteromedial nucleus (VPM) of the thalamus, whereas paralemniscal fibers originate in the posteromedial nucleus (POm). While these 2 TC projections are largely complementary in L4, overlap in other cortical layers is still a matter of debate. VPM and POm axons were specifically labeled in the same rat by virus-mediated expression of different fluorescent proteins. We show that columnar and septal projection patterns are maintained throughout most of the cortical depth with a lower degree of separation in infragranular layers, where TC axons form bands along rows. Finally, we present anatomical dimensions of "TC projection domains" for a standard column in S1.

Keywords: AAV, cortical column, POm, thalamocortical, VPM

Introduction

Peripheral sensory stimuli are conveyed to primary sensory cortex mainly via thalamic nuclei. Thalamocortical (TC) axonal projections have been extensively studied ever since the first drawings of Cajal (Cajal 1904) and Lorente de Nó (Lorente de Nó 1922, 1938). Anatomical studies have qualitatively described the spatial distribution of TC afferents (Lorente de Nó 1938; Jones and Powell 1970; Killackey 1973; White 1979; Herkenham 1980; Chmielowska et al. 1989; Lu and Lin 1993), and recent physiological investigation has provided insight into the strength, convergence, and synchrony of TC connections (Bruno and Sakmann 2006). However, a quantitative assessment of the expected number of synaptic contacts made between TC axons from different thalamic nuclei and cortical neurons is still largely missing. We have therefore attempted to estimate the anatomical determinants of TC input to excitatory neurons in the primary somatosensory cortex (S1) of the rat by measuring 1) TC axonal projections using virus-mediated expression of fluorescent proteins, 2) the number and distribution of neuronal somata in an entire cortical column, and 3) the dendritic geometry of 7 types of excitatory neurons in a cortical column. These studies are reported in this and the subsequent 2 articles (Meyer, Wimmer, Hemberger, et al. 2010; Meyer, Wimmer, Oberlaender, et al. 2010).

TC axon projections to S1 are divided into anatomically separated pathways (Lorente de Nó 1949), referred to as the lemniscal (specific and somatosensory) projection arising from ventral posteromedial nucleus (VPM) cells and the paralemniscal (global and multisensory) projection from posteromedial nucleus (POm) cells (Jones 2002). These 2 TC projections are known to concentrate vertically in different layers and horizontally in "barrels" or "septa" (Woolsey and Van der Loos 1970; Jensen and Killackey 1987; Koralek et al. 1988; Chmielowska et al. 1989; Agmon et al. 1993; Lu and Lin 1993; Bureau et al. 2006; Alloway 2008; Petreanu et al. 2009). The exact degree to which the 2 pathways innervate different cortical layers and different classes of target cells is still a matter of debate. Potentially both TC projections overlap and innervate the same class of target cells (Ahissar et al. 2001; Yu et al. 2006; Lubke and Feldmeyer 2007). The degree of overlap is an important issue because of questions related to near simultaneous versus sequential TC activation of cortex (Armstrong-James et al. 1992; de Kock et al. 2007).

Whole-cell recordings from post hoc reconstructed L2/3 pyramidal cells in S1 suggested that in supragranular layers, the excitatory neurons are functionally segregated according to the location of their somata with respect to barrels and septa in the granular layer apparent in cytochrome oxidase (CO) stained sections (Brecht et al. 2003). "Column-related" pyramids in L2/3, located above the barrels, are more responsive to whisker deflection than the "septum-related" pyramids that are located above the septa (Brecht et al. 2003). The functional separation of pyramids with reference to their position in the tangential plane suggested that in the supragranular and granular layer, lemniscal and paralemniscal pathways may remain separate and innervate different cell populations (Bureau et al. 2006; Kerr et al. 2007). In infragranular layers, slender-tufted and thick-tufted pyramids seem to segregate less clearly into column-related and septum-related subpopulations, respectively (Manns et al. 2004). Receptive fields (RFs) of both thick-tufted pyramids and L6 neurons are multiwhisker and elongated in the row direction (Manns et al. 2004; de Kock et al. 2007). These differences in response to whisker deflection could, at least in part, be due to

the pattern of TC-axonal arborizations in the cortex, in addition to the wider dendritic spread of infragranular pyramids.

We mapped the density of projections of VPM and POm axonal arbors and their presynaptic terminals through the depth of the cortex using cytoplasmic- or bouton-specific fluorescent protein (FP). The results show that VPM and POm axons form vertically oriented bundles that are in register with L4 barrels and septa, respectively. Both TC projections complement each other throughout the cortical depth, defining a column divided into layers and sublayers innervated to different degrees by VPM and POm. We define a standard "TC projection column" based on TC axon projection patterns.

Materials and Methods

P28 Wistar rats (80–120 g body weight) were used for virus injection into VPM and POm, respectively. Adenoassociated virus 1/2 (AAV1/2) expressing FP was microinjected stereotaxically into either of the 2 thalamic nuclei. CCD-camera epifluorescence microscopy and confocal laser scanning microscopy were used to quantify the areal and laminar density of VPM and POm projections in the barrel field.

Virus Particles
Virus particles for AAV1/2-humanized renilla green fluorescent protein were obtained from M. During (infective titer $1 \cdot \times 10^9$ cells/mL; Klugmann et al. 2005). Furthermore, we generated AAV1/2-monomeric red fluorescent protein (mRFP), AAV1/2-mOrange, AAV1/2-enhanced GFP (EGFP), and AAV1/2-synaptophysin-EGFP preparations (titer 8×10^6–8×10^7 PFU/mL) using helper plasmids encoding cap1 and cap2 at a ratio of 1:1 (Grimm et al. 2003). Transcription from all AAV constructs was controlled by a hybrid cytomegalovirus enhancer/chicken β-actin promoter (Fitzsimons et al. 2002). Biosafety: All experiments were carried out according to biosafety level 1 guidelines specified in the German GenTSV.

Depending on the individual virus preparation used, 78–95% of thalamic neurons in the injected area were infected as assessed by comparing the number of FP-expressing cells with the total number of neurons identified by immunocytochemistry (mouse anti-NeuN antibody; Millipore; dilution 1:1000, data not shown). The size of the homogenously infected focus typically had a radius of ~500 μm.

Stereotaxic Injections

Anesthesia
Experiments were conducted in accordance with the German animal welfare guidelines. Rats were anesthetized by intraperitoneal injection of 6.5 μL/g body weight of a mix of 20 μL fentanyl (0.0785 mg/mL), 80 μL midazolam (5 mg/mL), and 30 μL medetomidin (1 mg/mL) diluted 10-fold with sterile water. Rectal body temperature was maintained at 37–37.5 °C with a heating pad. After skin suturing, anesthesia was terminated by subcutaneous injection of 2.45 μL/g body weight of 120 μL naloxon (fentanyl antagonist, 0.4 mg/mL), 800 μL flumazenil (midazolam antagonist, 0.1 mg/mL), and 60 μL atipamezol (medetomidin antagonist, 5 mg/ mL).

Stereotaxic injections were performed as described previously (Wimmer et al. 2004). In brief, the SAS75 stereotaxic alignment system was used in combination with the EM70G manipulator (Kopf Instruments). This alignment system permits precise adjustments of the head in all 3 axes prior to injection. To achieve maximal precision in aligning the head horizontally, an electronic leveling device (eLeVeLeR) was used which permits highly precise leveling (Wimmer et al. 2004). Coordinates for VPM: 2.85 mm posterior of bregma, 3.2 mm lateral of the midline, and 5.05 mm deep from the pia. Coordinates for POm: 3.25 mm posterior, 2.1 mm lateral, and 5.2 mm deep.

Craniotomies with a diameter of approximately 0.5 mm were drilled above the injection sites. Injection capillaries (~1 cm length) with an outer tip diameter of 12-15 μm were pulled on a P87 horizontal puller (Sutter Company) using calibrated micropipettes (5 μL, intraMARK; Blaubrand). The calibration was used to estimate the injected volume that was between 50 and 200 nL.

Preparation of Paraformaldehyde-Fixed Brain Slices and Staining Methods
Rats were anesthetized with a lethal dose of urethane and transcardially perfused with 15 mL 0.1M phosphate buffer (PB) followed by 15 mL PB with 4% paraformaldehyde (PFA), 8 to 21 days after virus delivery. The brain was extracted and incubated overnight in PB containing 4% PFA at 4 °C. Tangential or TC (45° from midline) vibratome sections with 50–100 μm thickness were prepared (Bernardo and Woolsey 1987; Agmon and Connors 1991; Fleidervish et al. 1998).

Single TC axons were filled juxtasomally with biocytin (Pinault 1996). Biocytin was visualized in fixed brain slices after 3-h incubation in PBS with Streptavidin–Alexa594 (Invitrogen) and 0.3% TritonX-100. Subsequently, sections were washed in PB and mounted on glass slides using SlowFade light mounting medium (Invitrogen).

Confocal Microscopy
Confocal image stacks of PFA-fixed brain slices were acquired with a Leica TCS SP2 laser scanning microscope with 488 nm (EGFP) and 568 nm (mRFP) laser wavelengths and ×10 (HC PL APO CS; NA 0.40), ×40 (HCX PL APO CS; NA 1.25; oil immersion), or ×63 (HCX PL APO CS; N.A. 1.32, oil immersion) Leica objectives. Mosaic scans were done using a motorized x-y stage (Maerzhaeuser). Confocal images are maximum projections of stacks generated using the Leica TCS software or Volocity (Improvision).

Fluorescence Microscopy
Epifluorescence images were obtained using an Olympus BX-51 upright microscope equipped with GFP (excitation 488 nm, emission 520 nm) and Alexa594 (excitation 543 nm, emission 600 nm) fluorescence filter sets. A mercury lamp was used for illumination. Epifluorescence images were taken with ×4 and ×10 air objectives (NA 0.1 and 0.25, respectively). Pixel size of TIFF images was 3.4×3.4 μm.

Anatomical Landmarks of VPM and POm Projections
Slices from different age-matched rats were selected in the same anterior–posterior region and dorsomedial area of the cortex and were aligned with respect to pia, the border between L4 and L5 as defined by NeuN staining and subcortical white matter (SCWM; Meyer, Wimmer, Oberlaender, et al. 2010). Serial tangential sections were aligned according to the pattern of vertically oriented blood vessels.

For determination of the dimensions of a projection column in TC sections, we used the brains of 12 animals (7 virus injections into VPM and 5 injections into POm). For measurements in tangential sections, we used the brains of 9 animals with POm virus injections and 20 animals with injections in VPM. All measurements of distances and areas of barrels and septa were made after outlining anatomical landmarks on fluorescence images photographed at ×2-20 magnification (see above). Pia and SCWM outlines and distance or area measurements were done using the analySIS program package (Olympus) on images taken at ×2 or ×4 magnification (pixel size see above). AnalySIS was also used to manually draw the borders of fluorescent structures formed by the septa or laminar bands. If necessary, fluorescence images were overlaid with the brightfield image of the same section. We used these outlines of cortical surface (pia) and SCWM as well as "drop-like" structures and hollows in TC and tangential sections to make dimension measurements. For the barrel or hollow centers, 2 lines along the row and along the arc were drawn by eye, and the intersection of these 2 lines was taken as center of barrel or hollow, respectively. These were used to determine distances between neighboring barrel and hollow centers. Determination of borders of structures in fluorescent images is, however, somewhat
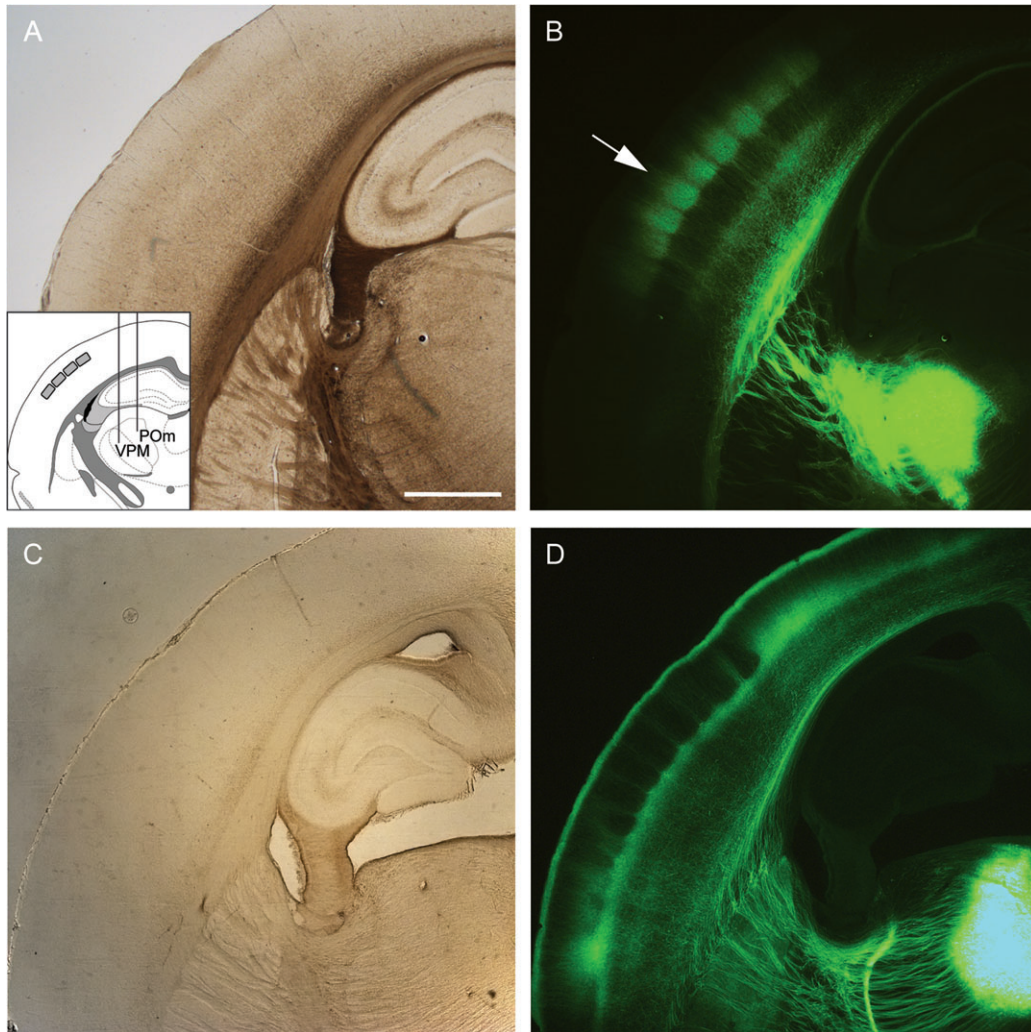
Figure 1. TC projections from VPM and POm to S1. (*A*) Brightfield image of a TC section that includes part of the barrel field. Inset: Schematic drawing of specific stereotaxic injection into VPM and POm, respectively. (*B*) Bulk labeling of VPM axons, epifluorescence image of the TC section shown in *A*. Arrow: drop-like structures defined by VPM projections. (*C*) Brightfield image of TC section from a different animal with AAV injection into POm. (*D*) Bulk labeling of POm axons, same section as shown in *C*. Scale bar 1 mm.
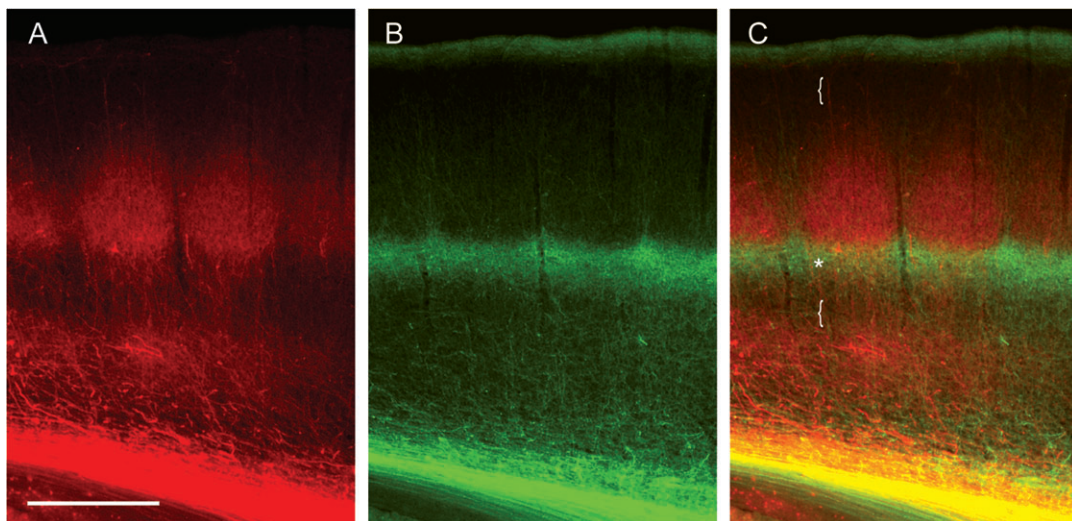

Figure 2. Dual labeling of VPM and POm axons. Labeling of VPM and POm axons in the same animal by AAV-mediated expression of different fluorescent proteins. (*A*) VPM projections (mRFP; red) in a TC slice. (*B*) POm projections (EGFP; green). (*C*) Merge of A and B, illustrating afferent sparse zones of low fluorescence (braces). Potential overlap of VPM and POm axon fluorescence in the deeper portion of barrels (yellow, asterisk). Scale bar 500 µm.
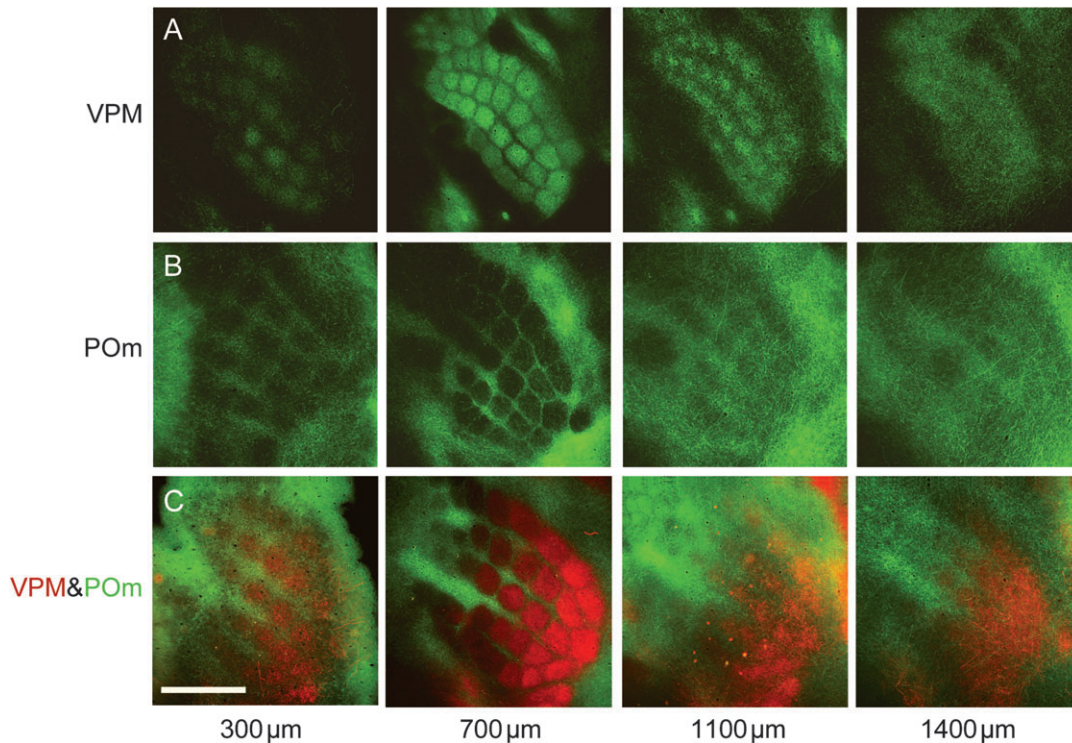
Figure 3. VPM and POm projections span most of the cortex width and complement each other. Tangential sections at different depths as indicated. (*A*) VPM axons. (*B*) POm axons. (*C*) Two-color labeling of VPM and POm axons in the same animal by expression of 2 different fluorescent proteins illustrates complementary projection patterns (VPM: red; POm: green; Koralek et al. 1988).

subjective because borders do not appear sharp at higher magnifications (e.g., ×10 or ×20 magnification). Dimensions of the cortical projection columns were predominantly based on measurements of arc 2 and arc 3, which are located above the hippocampal CA3 region (arc 1 are the straddlers). In few cases (Fig. 6), measurements were also performed on arcs anterior of the HC-CA3 region.

Line plots of synaptic density along and across column axes were prepared using ImageJ (http://rsbweb.nih.gov/ij/) after background correction and Gaussian filtering of confocal mosaic scans.

Statistical Analysis

In boxplots, the gray box represents the 25th-75th percentile, the long vertical lines the 10th-90th percentiles (only when $n > 10$ observations), and the dark horizontal line the median. Graphpad Instat 3 was used for statistical analysis on distributions of Figures 5 and 6. First, we used the Kolmogorov-Smirnov test that indicated that our data were normally distributed. Subsequently, we used analysis of variance (ANOVA) (with Tukey posttest) to test for significant differences in cross-sectional area of different barrel columns (Figs 5*D* and 6*D*) and to test for significant differences in distance between barrel centers within rows or between arcs (Figs 5*E* and 6*E*). Significance level was set at $P < 0.05$.

Results

Viral expression of fluorescent tracers allows purely anterograde labeling with no contamination of retrogradely filled corticothalamic cells, which commonly occurs with conventional tracers (Chmielowska et al. 1989). Locally restricted virus injections were made either into VPM or POm (Fig. 1*A* inset). Figure 1*B,D* illustrates the differences in projection patterns of lemniscal and paralemniscal axons in the cortex, depending on whether the virus injection was made in VPM or POm. These TC "projection domains" in S1 only partly respect

the delimitations of layers or barrels and sometimes extend across barrel borders defined by cortical cytoarchitecture. Therefore, we used a terminology different from previously established definitions of layers and columns to help distinguish TC projection domains as specific functional units with a common input.

We analyzed barrel cortex regions associated with macrovibrissae of arc numbers (1–6) in C–E rows. These are located above the lateral ventricle/hippocampal fornix region in the dorsomedial area of S1.

Vertical Architecture of VPM and POm Projections

VPM axons arising from bundles in the stria enter the SCWM and bend into a tangential direction almost parallel to the pia (Bernardo and Woolsey 1987, Fig. 1*B*). Axons then turn again to enter the cortex along an axis perpendicular to the pia (Bernardo and Woolsey 1987, Figs 1*B* and 2*A*). The density of vertically and tangentially oriented axon branches within the cortex is inhomogeneous and depends on the distance from the pia (Chmielowska et al. 1989; Jhaveri et al. 1991). High densities of axon branches, often oriented tangentially, give rise to 2 irregularly delineated "bands" of high fluorescence that are oriented in parallel to the pia (Frost and Caviness 1980; Chmielowska et al. 1989; Jhaveri et al. 1991; Agmon et al. 1993, Figs 1*B* and 2*A*). The first band is located at a distance of ~1150-1400 μm from the pia (VPM band 1); the second, more intense band extends from ~300 to ~800 μm depth from the pia (VPM band 2). Within the upper band regularly spaced drop-like structures can be seen (Fig. 1*B*, arrow; Fig. 2*A*). The middle portion of each drop extends closer to the pia.

Figure 1*D* illustrates the different appearance of vertically oriented POm axon arbors in the cortex (Lu and Lin 1993;

Alloway et al. 2004). They form 2 tangentially oriented bands of high fluorescence. POm band 1 is located between ~800 and ~1000 μm and POm band 2 extends from the pia down to ~120 μm. POm band 1 is not homogenous but is characterized by regularly spaced triangular structures from which vertically oriented axon bundles extend toward the pia, forming the septa (Koralek et al. 1988; Lu and Lin 1993; Alloway et al. 2004; Kichula and Huntley 2008, Fig. 1D). Close to the pia, the vertically oriented POm axons bend into the tangential plane and form POm band 1 underneath the pia.

The 2 fluorescence images in Figure 1B,D were taken from TC slices from 2 different cortices, one with VPM and the other with POm specific axon labeling. These images suggest a possible overlap of VPM and POm projections at a depth of ~800–1000 μm underneath the pia. Furthermore, the images suggest that 2 regions of the cortex are only sparsely innervated by both the VPM or POm axons. These "afferent sparse zones" are located at a depth of ~100–300 μm and ~1000–1150 μm from the pia below the deeper POm axon band.

Dual VPM and POm Labeling Reveals Afferent Sparse Zones

To delineate the complementing dual TC projections more clearly, we labeled VPM and POm axons in the same animal by injecting 2 different types of virus into VPM and POm, respectively. These viruses expressed fluorescent proteins emitting light at different wavelength (mRFP and EGFP; VPM axons in red, POm axons in green) and allowed direct comparison of VPM and POm innervation patterns within the same cortex (Fig. 2A,B). Differences in laminar distribution of VPM (Fig. 2A) and POm axons (Fig. 2B) are readily apparent. Regions of potential overlap between VPM and POm bands exist at a depth of 800–1000 μm as seen in the merged image (Fig. 2C, asterisk). Afferent sparse zones are apparent at a depth of ~100–300 μm from the pia (corresponding to L2) and below ~1000 μm depth (including the lower half of L5A and the upper half of L5B; Fig. 2C, braces).

Tangential Architecture of VPM and POm Axons

In tangential sections, it becomes obvious that the vertically oriented architecture of VPM axon bundles is most clearly delineated at ~700–800 μm depth (Killackey and Leshin 1975; Caviness and Frost 1980) and is maintained throughout most of the cortical depth between ~300 and ~1100 μm (Fig. 3A). Sequential tangential sections beginning in the supragranular layers and progressing to deeper layers show that column-like axon bundling appears at 300 μm depth and continues down to a depth of ~1100 μm (Figs 3A and 4). Remarkably, from ~1200 μm depth and deeper the axon branches are organized mostly in rows and low fluorescence regions separating columns within the rows almost disappear (Figs 3 and 4). Due to the curvature of the barrel cortex, sections are not always perpendicular to the z-axis of a column. Therefore, the distribution of VPM and POm fluorescence at 1100 and 1400 μm depth looks slightly asymmetric. Nevertheless, the row-like organization of the projections is apparent. Fluorescence intensity profiles in the arc direction show clear peaks and valleys, whereas profiles in the row direction lack these (Fig. 4, asterisks).

The honeycomb pattern of POm projections in the tangential plane is most clearly delineated at ~700 μm depth (Fig. 3B). The
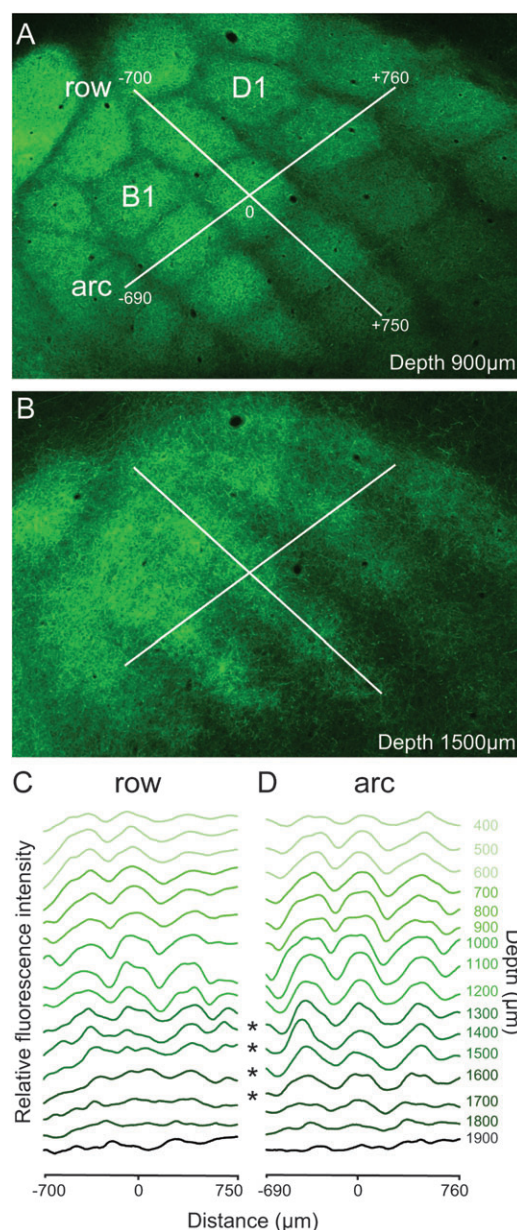

Figure 4. VPM projections form rows in infragranular cortical layers. (A) Fluorescence image of tangential section at ~900 μm depth. Lines indicate regions of interest (ROIs) along C-row (shown in aligned serial sections in C) and arc 2 (shown in D). (B) Tangential section at ~1500 μm depth with ROIs projected down from L4. (C) Fluorescence intensity profiles along C-row throughout the depth of the cortex measured in serial tangential sections aligned using radial blood vessels. (D) Analogous to C but along arc 2. Asterisks indicate that in infragranular layers fluorescence profiles show peaks and valleys along arcs but not along rows.

POm projections maintain this pattern also in cortical layers that are closer to the pia (at 300 μm depth, Fig. 3B), and surprisingly also in deeper portions (1100 μm from the pia, Fig. 3B). Even at 1400 μm depth, the POm projections are still patterned, however, as a predominantly row-like structure.

Dual virus injections into VPM and POm demonstrate that POm axon branches largely avoid the area occupied by VPM axons at all depth throughout most portions of the cortex width (Fig. 3C). Thus, the POm axon domains are complementing the VPM axon domains (Koralek et al. 1988; Kichula and Huntley 2008), spanning cortical depth from ~300 to ~1400 μm.

Overlaps between the 2 axon projections are expected at 800–1000 μm. Here, vertically oriented VPM axon bundles cross the horizontally oriented lateral axons of the POm and intermingle (Fig. 2C).

Dimensions of VPM and POm Axon Fields

The projection patterns of VPM or POm axons measured in different cortices define the volume of a "standard projection column" characterized by its average cross-sectional area and length between pia and SCWM. We defined this standard column using the maximal density VPM projection at 700–900 μm depth as cross-sectional area. Pia and the upper border of the SCWM (excluding the axons of SCWM) demarcate the length of a projection column along the vertical z-axis. The size of a projection column as defined by the dimensions of VPM and POm axons (see below) is also dependent on the topographical row and arc location of the

column (Woolsey and Van der Loos 1970). Axons from VPM barreloids linked to the long caudal (low arc number) whiskers project to the posteriomedial subfield of the barrel cortex, while the short rostral whiskers are linked to the anterolateral subfield. For determining the dimensions of projections columns, we identified the numbers of row and arcs in TC slices by their relative proximity to hippocampal fornix and CA3 region (Figs 5A and 6A).

VPM Projections

The mean width of the cortex (pia to SCWM) in our material with VPM injections was 1739 μm for columns in arc 1–3, 1782 μm for arc 2 and 3 columns, and 1840 μm for all columns (arc 1–6; $n = 7$; Fig. 5C). The mean distance from pia to lower border of VPM band 2 was 790 μm, 798 μm, and 801 μm, for columns in arc 1–3, arc 2 and 3, and all columns, respectively (Fig. 5C). The corresponding average distance between pia and
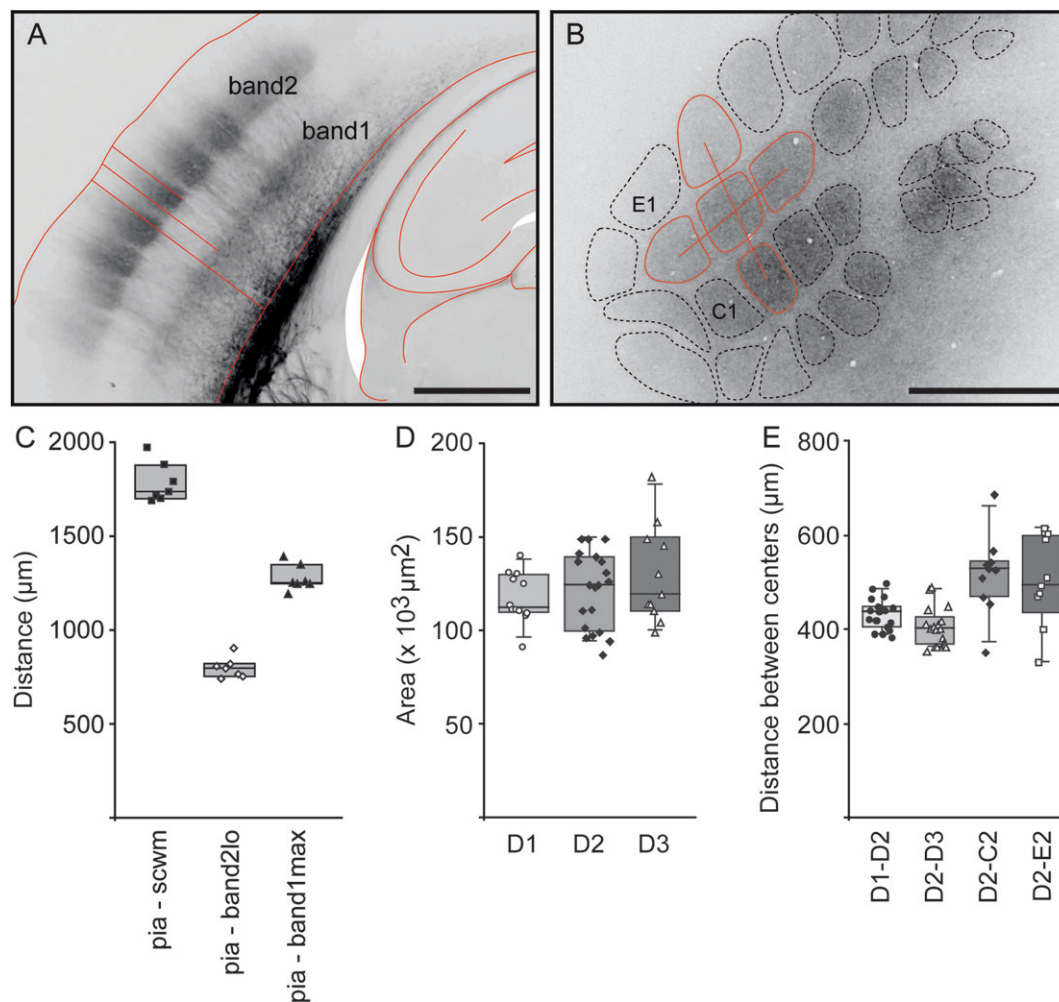

Figure 5. Landmarks and dimensions of VPM projections. (A) Fluorescence image of VPM projection pattern in a TC section. Anatomical landmarks of VPM projections in cortex are pia and SCWM, indicated as red outlines. The VPM projections form 2 tangential bands referred to as VPM band1 (closer to the SCWM) and VPM band2 (closer to the pia). Distances analyzed for C are indicated as red lines: pia–SCWM, pia-band2lo (i.e., lower edge of band2), pia-band1max (i.e., the maximum of band1). Another band close to the SCWM was not quantified as it does not appear with bouton-specific labeling. Scale bar 1 mm. (B) Fluorescence image of VPM projection pattern in a tangential section at 800 μm depth. Here, anatomical landmarks are the cross-sectional area of VPM axon arbor outline and the distances between "centers of mass" of barrel border outlines as indicated by red lines. Scale bar 1 mm. (C) Distances between landmarks for columns in arc 2 and 3 as measured in 7 TC sections. Mean distances: pia–SCWM 1782 μm (range 1688–1970 μm), pia-band2lo 798 μm (range 740–901 μm) and pia-band2max 1277 μm (range 1194–1390 μm). (D) Cross-sectional area of the D1, D2, and D3 projection column (ANOVA, $P = 0.35$). (E) Center-to-center distances between VPM projection to the D2 column and 4 of its surround columns as indicated. Measurements were made using sections at 700–900 μm depth from pia.
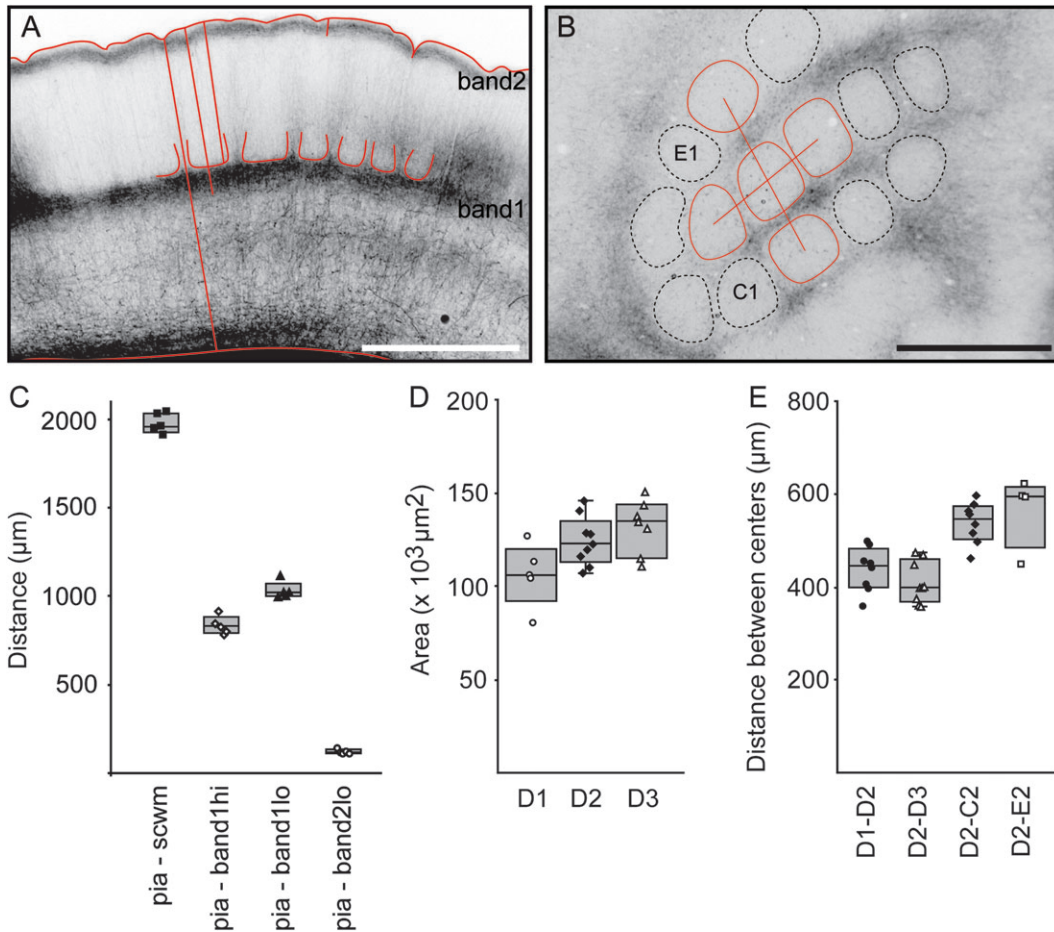
Figure 6. Landmarks and dimensions of POm projections. (A) Fluorescence image of POm projection pattern in a TC section. The POm projections form 2 POm innervation bands, POm band1 (closer to the SCWM), and POm band2 (underneath pia). Distances measured for C are indicated as red lines: pia–SCWM, pia-band1hi, pia-band1lo, and pia-band2lo. Scale bar 1 mm. (B) Fluorescence image of POm projection pattern in a tangential section at 900 μm depth. Anatomical landmarks used were the outlines of hollows to determine the cross-sectional area and the mean distances between the centers of hollows as indicated by red lines. Scale bar 1 mm. (C) Distances between landmarks of POm projections (n = 5). Mean distances: pia–SCWM 1977 μm (range 1908–2042 μm), pia-band1hi 834 μm (range 780–914 μm), pia-band1lo 1031 μm (range 996–1116 μm), and pia - band2 116 μm (range 106–140). (D) Cross-sectional area of the D1, D2, and D3 hollows (ANOVA, P = 0.02; Tukey, P < 0.05). (E) Center-to-center distance between 4 of the hollows surrounding D2.

the maximum of the deep VPM band 1 was 1264, 1277, and 1300 μm, respectively (Fig. 5C shows measurements only for columns in arc 2 and 3).

The cross-sectional area of the maximal density VPM projection was determined in tangential sections (Fig. 5B). The average area varied slightly with the topographic location at the column in the barrel field (Fig. 5D). For D2 columns, the average cross-sectional area is ~12 1000 μm^2 (n = 20, Fig. 5D). Cross-sectional areas shown in Figure 5D are not significantly different between columns (ANOVA, P = 0.35). Mean distances between centers of VPM cross-sections around the D2 column vary between 403 and 517 μm (Fig. 5E).

POm Projections
In TC sections, the upper halves of columns appear as hollows that are separated by thin vertically oriented POm septa (Fig. 3). The average distances between 2 different landmarks designated as POm bands 1 and 2 are shown in Figure 6C. The mean pia–SCWM distance in this data set was 1977 μm (Fig. 6C). POm band 1 in the middle portion of the cortex is located between 834 and 1031 μm, POm band 2 extends from the pia down to 116 μm depth (Fig. 6C).

The laminar geometry of POm architecture was measured in tangential sections at ~800 μm depth (Fig. 6B). The mean cross-sectional area of the D1-D3 hollows is ~12 4000 μm^2 (Fig. 6D). The mean distances between center of hollows above the barrel and within the D row vary between 438 and 566 μm (Fig. 6E).

In summary, quantification of VPM and POm architecture yields comparable estimates for the cross-sectional area and length of a projection column (average cross-sectional area for D2: VPM projection 12 1000 μm^2, POm projection 12 4000 μm^2; average length of all columns analyzed VPM data set 1840 μm; POm data set 1977 μm). While the volume of a projection column depends on its topographical location within the barrel field, we defined a "standard column" using 12 1000 μm^2 cross-sectional area and 1840 μm length. The volume of this standard column is ~0.22 mm^3.

Large Caliber Axons
A peculiarity of the axon bundles in the septa following virus deposit in the POm is the occurrence of "large caliber" axons with diameters of up to 4 μm (Fig. 7A). These bend into the
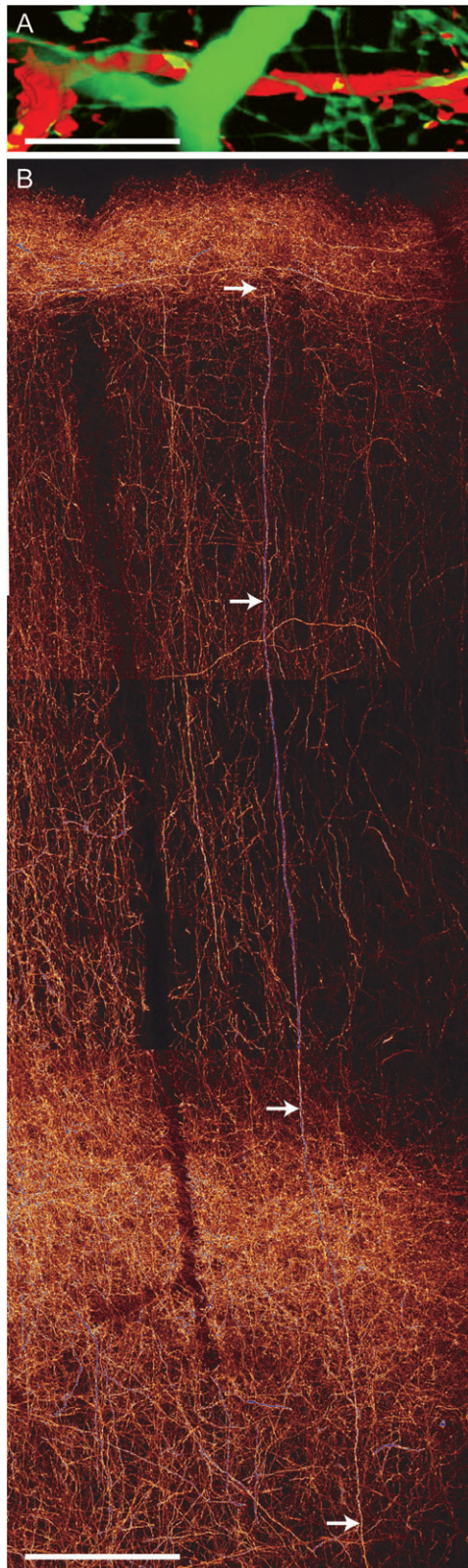
Figure 7. Large caliber axons: highway to the cortex? (*A*) High-magnification image of a large caliber axon branch segment in L1. Green: giant POm axon; red: apical dendrite of an infragranular pyramidal cell labeled with biocytin–streptavidin–Alexa594. Scale bar 10 μm. (*B*) Reconstruction of a large caliber axon extending from SCWM to L1 (arrows). The image represents a montage of maximum projections of confocal stacks. Scale bar 100 μm.

tangential plane at ~80 μm distance from the pia. They then extend over hundreds of μm along the cortical surface (Fig. 7*B*). In 100 μm thick TC sections, we observed on average 17–20 of these thick axons per individual column (*n* = 11). In tangential sections deeper than 100 μm from the pia, the large caliber axons stand out as bright puncta (not shown).

Distribution of Synaptic Boutons of VPM and POm Axons
Functionally, the most important structure of VPM and POm projections are their synaptic boutons. Their distribution was measured by expressing GFP-tagged synaptophysin, a presynaptic marker specific for vesicles in boutons (Leube et al. 1987; Silver and Stryker 1999). Vertical and areal densities were quantified by densitometry of GFP fluorescence.

Bouton Specificity
Figure 8*A* confirms the specificity of bouton labeling using GFP-tagged synaptophysin. Confocal imaging of an axon branch filled with biocytin (visualized using streptavidin–Alexa594; Fig. 8*A*, red) illustrates that the green puncta representing synaptic vesicle clusters are specifically associated with axonal swellings (variscosities) characteristic of presynapses (Fig. 8*A*1,*A*2). Vice versa, we did not observe green puncta not associated with an axonal swelling.

Vertical and Tangential Density Profiles
The differential distribution of bouton density of the 2 projection systems is apparent following a virus injection into either VPM (Fig. 8*B*) or POm (Fig. 8*C*). The tangentially oriented bands appear sharper than those seen with axonal labeling. The difference in the laminar distribution of VPM and POm boutons is, as expected, largest in the middle portion of the cortex. Again, the distribution of VPM boutons at less than 800 μm depth resembles the shape of a drop extending up to the pia. The distribution of POm bouton fluorescence reveals triangular structures at the base of the hollows.

Depth profiles along the *z*-axis measured by fluorescence densitometry of VPM or POm boutons were compared in corresponding TC sections from different animals. We quantified bouton densities along the central vertical column axis throughout the depth of the cortex. The superposition of VPM and POm bouton fluorescence profiles (Fig. 9*A–D*) indicates several regions of overlap of VPM and POm boutons (Fig. 9*B*). However, the overlap of synapse-specific VPM and POm labeling seems to be less extensive than for axonal labeling (see Fig. 2*C*, asterisk).

Tangential density scans were made at 2 different distances from the pia at 700 and 1250 μm for VPM (Fig. 8*E*) and POm boutons (Fig. 8*F*). Columns and septa are most sharply delineated at 700 μm depth, resulting in clear separation between barrel and septum in horizontal density profiles (Fig. 9*E/F*, arrows).

Discussion

Bulk labeling of TC axons using cytoplasmic- or bouton-specific GFP shows that VPM and POm projections establish vertical axon bundles in the vibrissal cortex. These bundles span almost the entire width of the cortex. They extend from ~100 μm above the L6/SCWM border to about 20–30 μm underneath the pia. At light microscopic level, both projections complement
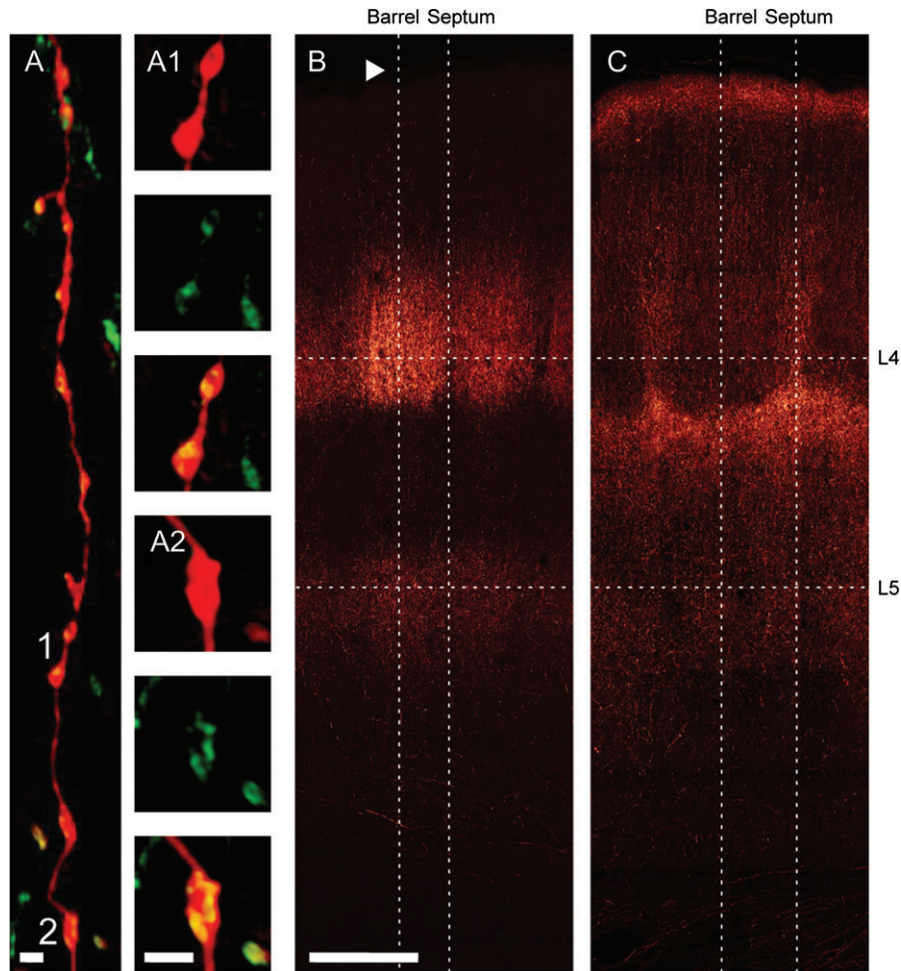
Figure 8. Bouton distributions of VPM and POm define borders of columns and septa. (*A*) VPM axon with synaptophysin-EGFP–labeled presynaptic boutons and biocytin-volume fill (streptavidin–Alexa594 detection). Vesicle clusters are exclusively associated with axonal varicosities. 3D reconstruction of a confocal stack. (*A1, A2*) Higher magnification images of the 2 single boutons indicated in *A* as 1 and 2, respectively. Top image in each panel illustrates the axonal volume fill, middle image shows the vesicle cluster, and the bottom image is an overlay of both. Scale bars 1 μm. (*B*) Maximum projection of a confocal stack showing bouton distribution after VPM injection of AAV-synaptophysin-EGFP. Dotted lines indicate scan lines for calculating bouton density profiles in the vertical (column and septum axes) and horizontal plane (L4 and L5), respectively (see Fig. 9). Arrow indicates pia. (*C*) As *B* but after POm injection of AAV-synaptophysin-EGFP. Scale bar 250 μm.

each other throughout most portions of the cortex while they occupy the same cortical volume at 800–1000 μm depth and, to a smaller degree, also in deep infragranular layers, indicating regions of potential overlap where the 2 TC projections may innervate the same cortical target neurons (Meyer, Wimmer, Hemberger, et al. 2010). Finally, 2 afferent sparse domains appear in supra- and infragranular layers, respectively. The data presented here confirm some findings from prior work on the topography of TC axons (Killackey and Leshin 1975; White and DeAmicis 1977; Caviness and Frost 1980; Frost and Caviness 1980; Koralek et al. 1988; Chmielowska et al. 1989; Fabri and Burton 1991; Agmon et al. 1993; Lu and Lin 1993; Bureau et al. 2006; Kichula and Huntley 2008; Petreanu et al. 2009) but also reveal previously unknown details on TC innervation.

VPM Projection Domains

In each column, VPM axons form tangential bands with high density of lateral branching that are located at a depth of ~1150–1400 μm and ~300–800 μm, respectively. Just above the SCWM, axons entering the cortex via the stria change their directions. Therefore, axon bundling is not obvious in this plane of sectioning. In the supragranular portion, VPM axons form a drop-like structure, with the tip pointing toward the pia in the middle of the column. Therefore, L3 pyramidal neurons are likely to be directly innervated by VPM and not entirely dependent on L4 for afferent input. VPM axon domains of different columns are well separated from each other between ~300 and ~1100 μm depth. Deeper in the cortex (~1200–1700 μm), TC axon domains are almost confluent in the row direction, but they remain separated in the arc direction. This row-like organization of TC afferents might explain why RFs of pyramidal neurons in infragranular layers are predominantly oriented along the rows (Manns et al. 2004; de Kock et al. 2007) and may also account for the fact that thick-tufted pyramids have multiwhisker RFs (de Kock et al. 2007), in addition to a possible multiwhisker innervation of these cells.

Visualization of TC boutons by virus-mediated expression of synaptophysin–EGFP allowed analysis of TC synapse densities across layers. Synaptophysin–EGFP fluorescence density distributions are more sharply delimited than axonal densities. The distribution of boutons is probably more meaningful for
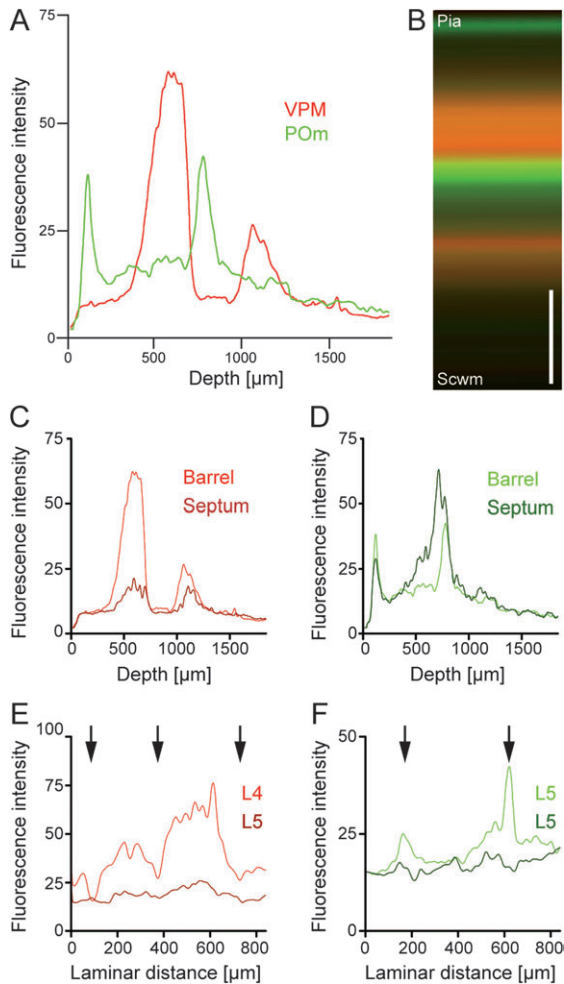
Figure 9. Bouton density profiles of VPM and POm projections reveal overlap domains. (*A*) Vertical column profiles of VPM (red line) and POm (green line) bouton fluorescence intensity (in relative units) measured in TC slices between pia and SCWM. Boutons were labeled as described in Figure 8. (*B*) Separation and overlap of VPM and POm projections in a column. Merged profiles of VPM (red) and POm bouton (green) projections illustrate well separated and partially overlapping projection domains (yellow) of VPM and POm boutons at different depths. Two afferent sparse zones are also apparent. Total length between pia and SCWM is normalized to "standard length" 1840 μm VPM bouton in red and POm bouton profile in green. Scale bar 0.5 mm. (*C*) VPM bouton profiles along vertical column axis (bright red) and septum (dark red). (*D*) POm bouton profiles along vertical column axis (bright green) and septum (dark green). (*E*) Horizontal profiles across column borders for VPM boutons at 2 different depths from the pia as indicated in Figure 8. Individual fluorescence peaks are clearly separated by darker septa at ~750 μm depth (bright red; arrows). At 1200 μm depth, a weak laminar patterning is still present (dark red). (*F*) As E for POm boutons. At ~750 μm depth septa are clearly delineated (bright green, arrows). No clear separation between columns and septa is visible at 1200 μm depth (dark green).

delineating anatomical determinants of functional derivatives of TC innervation.

POm Projection Domains

POm axonal projections form vertical bundles branching into major horizontal bands located at ~800–1000 μm and ~0–120 μm depth from the pia. POm axons in the supragranular layer occupy the volume between VPM domains and "enclose" the drops that are occupied by the VPM axons. However, underneath these dense VPM projections, the POm projections extend well into the barrel column forming a sheath extending across the borders of columns. Here, the ascending vertical VPM axon arbors intermingle with the horizontal collaterals of POm axons.

A particular subtype of axons are the long-range large caliber axons. The location of the somata of these axons remains unknown. They may arise from POm cells that are innervated by axon collaterals of thick-tufted L5B cells via large calyx-type terminals located at their proximal dendritic excrescences (Veinante et al. 2000; Li et al. 2003; Groh et al. 2008). Similar axons have been described in the auditory cortex (Huang and Winer 2000). Their large diameters likely endow them with faster conduction velocities, and they are assumed to provide a high-speed connection between thalamus and cortex.

Dual Labeling of VPM and POm Axons

Using specific labeling of lemniscal and paralemniscal projections with fluorescent proteins in 2 different colors within the same tissue slice, we revealed an "overlap band" between 800 and 1000 μm depth and 2 afferent sparse zones, one in the supragranular layers (Keller et al. 1985; Lu and Lin 1993) and one in the infragranular layers, lacking intense axonal projections from either VPM or POm. Dendritic segments located in these afferent sparse zones are likely to be activated mostly via intracortical connections that may explain the weak responsiveness of a subset of L5 neurons to single-whisker stimulation (de Kock et al. 2007). The infragranular afferent sparse zone was not noted in previous studies (Lu and Lin 1993; Kichula and Huntley 2008) and may warrant future in vivo studies to investigate if there are 3 rather than 2 functional sublayers of L5.

Dimensions of a Standard Projection Column

On the basis of the outlines of these TC projections, one can define an anatomical standard projection column. This column is defined as a virtual cylindrical volume of cortical tissue that spans the width of the entire cortex (on average 1840 μm). This standard column has an average cross-sectional area of 12 1000 μm^2 and a volume of ~0.22 mm^3. A TC projection column is subdivided horizontally into shorter cylinders. These are innervated either by mostly one of the TC projections or by overlapping VPM and POm projections. The standard projection column can provide a basis for further analysis of anatomical determinants of thalamic input to S1 which is presented in the 2 subsequent articles (Meyer, Wimmer, Hemberger, et al. 2010; Meyer, Wimmer, Oberlaender, et al. 2010).

Funding

Notes

References

Agmon A, Connors BW. 1991. Thalamocortical responses of mouse somatosensory (barrel) cortex in vitro. Neuroscience. 41:365-379.
Agmon A, Yang LT, O'Dowd DK, Jones EG. 1993. Organized growth of thalamocortical axons from the deep tier of terminations into

layer IV of developing mouse barrel cortex. J Neurosci. 13:5365-5382.

Ahissar E, Sosnik R, Bagdasarian K, Haidarliu S. 2001. Temporal frequency of whisker movement. II. Laminar organization of cortical representations. J Neurophysiol. 86:354-367.

Alloway KD. 2008. Information processing streams in rodent barrel cortex: the differential functions of barrel and septal circuits. Cereb Cortex. 18:979-989.

Alloway KD, Zhang M, Chakrabarti S. 2004. Septal columns in rodent barrel cortex: functional circuits for modulating whisking behavior. J Comp Neurol. 480:299-309.

Armstrong-James M, Fox K, Das-Gupta A. 1992. Flow of excitation within rat barrel cortex on striking a single vibrissa. J Neurophysiol. 68:1345-1358.

Bernardo KL, Woolsey TA. 1987. Axonal trajectories between mouse somatosensory thalamus and cortex. J Comp Neurol. 258: 542-564.

Brecht M, Roth A, Sakmann B. 2003. Dynamic receptive fields of reconstructed pyramidal cells in layers 3 and 2 of rat somatosensory barrel cortex. J Physiol. 553:243-265.

Bruno RM, Sakmann B. 2006. Cortex is driven by weak but synchronously active thalamocortical synapses. Science. 312:1622-1627.

Bureau I, von Saint Paul F, Svoboda K. 2006. Interdigitated paralemniscal and lemniscal pathways in the mouse barrel cortex. PLoS Biol. 4:e382.

Cajal SR. 1904. Textura del sistema nervioso del hombre y de los vertebrados. N. Moya, Madrid, Vol. II, second part. English translation by T. Pasik and P. Pasik. Texture of the Nervous System of Man and the Vertebrates. Vol. III. New York: Springer.

Caviness VS, Jr., Frost DO. 1980. Tangential organization of thalamic projections to the neocortex in the mouse. J Comp Neurol. 194:335-367.

Chmielowska J, Carvell GE, Simons DJ. 1989. Spatial organization of thalamocortical and corticothalamic projection systems in the rat SmI barrel cortex. J Comp Neurol. 285:325-338.

de Kock CP, Bruno RM, Spors H, Sakmann B. 2007. Layer- and cell-type-specific suprathreshold stimulus representation in rat primary somatosensory cortex. J Physiol. 581:139-154.

Fabri M, Burton H. 1991. Topography of connections between primary somatosensory cortex and posterior complex in rat: a multiple fluorescent tracer study. Brain Res. 538:351-357.

Fitzsimons HL, Bland RJ, During MJ. 2002. Promoters and regulatory elements that improve adeno-associated virus transgene expression in the brain. Methods. 28:227-236.

Fleidervish IA, Binshtok AM, Gutnick MJ. 1998. Functionally distinct NMDA receptors mediate horizontal connectivity within layer 4 of mouse barrel cortex. Neuron. 21:1055-1065.

Frost DO, Caviness VS, Jr. 1980. Radial organization of thalamic projections to the neocortex in the mouse. J Comp Neurol. 194:369-393.

Grimm D, Kay MA, Kleinschmidt JA. 2003. Helper virus-free, optically controllable, and two-plasmid-based production of adeno-associated virus vectors of serotypes 1 to 6. Mol Ther. 7:839-850.

Groh A, de Kock CP, Wimmer VC, Sakmann B, Kuner T. 2008. Driver or coincidence detector: modal switch of a corticothalamic giant synapse controlled by spontaneous activity and short-term depression. J Neurosci. 28:9652-9663.

Herkenham M. 1980. Laminar organization of thalamic projections to the rat neocortex. Science. 207:532-535.

Huang CL, Winer JA. 2000. Auditory thalamocortical projections in the cat: laminar and areal patterns of input. J Comp Neurol. 427: 302-331.

Jensen KF, Killackey HP. 1987. Terminal arbors of axons projecting to the somatosensory cortex of the adult rat. I. The normal morphology of specific thalamocortical afferents. J Neurosci. 7:3529-3543.

Jhaveri S, Erzurumlu RS, Crossin K. 1991. Barrel construction in rodent neocortex: role of thalamic afferents versus extracellular matrix molecules. Proc Natl Acad Sci U S A. 88:4489-4493.

Jones EG. 2002. Thalamic organization and function after Cajal. Prog Brain Res. 136:333-357.

Jones EG, Powell TP. 1970. An anatomical study of converging sensory pathways within the cerebral cortex of the monkey. Brain. 93: 793-820.

Keller A, White EL, Cipolloni PB. 1985. The identification of thalamocortical axon terminals in barrels of mouse SmI cortex using immunohistochemistry of anterogradely transported lectin (Phaseolus vulgaris-leucoagglutinin). Brain Res. 343:159-165.

Kerr JN, de Kock CP, Greenberg DS, Bruno RM, Sakmann B, Helmchen F. 2007. Spatial organization of neuronal population responses in layer 2/3 of rat barrel cortex. J Neurosci. 27: 13316-13328.

Kichula EA, Huntley GW. 2008. Developmental and comparative aspects of posterior medial thalamocortical innervation of the barrel cortex in mice and rats. J Comp Neurol. 509:239-258.

Killackey HP. 1973. Anatomical evidence for cortical subdivisions based on vertically discrete thalamic projections from the ventral posterior nucleus to cortical barrels in the rat. Brain Res. 51:326-331.

Killackey HP, Leshin S. 1975. The organization of specific thalamocortical projections to the posteromedial barrel subfield of the rat somatic sensory cortex. Brain Res. 86:469-472.

Klugmann M, Symes CW, Leichtlein CB, Klaussner BK, Dunning J, Fong D, Young D, During MJ. 2005. AAV-mediated hippocampal expression of short and long Homer 1 proteins differentially affect cognition and seizure activity in adult rats. Mol Cell Neurosci. 28:347-360.

Koralek KA, Jensen KF, Killackey HP. 1988. Evidence for two complementary patterns of thalamic input to the rat somatosensory cortex. Brain Res. 463:346-351.

Leube RE, Kaiser P, Seiter A, Zimbelmann R, Franke WW, Rehm H, Knaus P, Prior P, Betz H, Reinke H, et al. 1987. Synaptophysin: molecular organization and mRNA expression as determined from cloned cDNA. EMBO J. 6:3261-3268.

Li J, Wang S, Bickford ME. 2003. Comparison of the ultrastructure of cortical and retinal terminals in the rat dorsal lateral geniculate and lateral posterior nuclei. J Comp Neurol. 460:394-409.

Lorente de Nó R. 1922. La corteza cerebral del rató n (Primera contribució n. La corteza acú stica). Trabajos del Laboratorio de Investigaciones Bioló gicas de la Universidad de Madrid.

Lorente de Nó L. 1938. The cerebral cortex: architecture, intracortical connections and motor projections. London: Oxford University Press. p. 291-339.

Lorente de Nó R. 1949. Cerebral cortex: architectonics, intracortical connections. In: Fulton J, editor. Physiology of the Nervous System. 3rd ed. Oxford, U.K: Oxford University Press. p. 274-301.

Lorente de Nó R. 1992. The cerebral cortex of the mouse (a first contribution-the "acoustic" cortex). Trans. A. Fairén, J. Regidor, L. Kruger. Somatosens Mot Res. 9:3-36.

Lu SM, Lin RC. 1993. Thalamic afferents of the rat barrel cortex: a light- and electron-microscopic study using Phaseolus vulgaris leucoagglutinin as an anterograde tracer. Somatosens Mot Res. 10:1-16.

Lubke J, Feldmeyer D. 2007. Excitatory signal flow and connectivity in a cortical column: focus on barrel cortex. Brain Struct Funct. 212:3-17.

Manns ID, Sakmann B, Brecht M. 2004. Sub- and suprathreshold receptive field properties of pyramidal neurones in layers 5A and 5B of rat somatosensory barrel cortex. J Physiol. 556:601-622.

Meyer H-S, Wimmer VC, Hemberger M, Bruno RM, de Kock CP, Frick A, Sakmann B, Helmstaedter M. 2010. Cell type-specific thalamic innervation in a column of rat vibrissal cortex. Cereb Cortex. doi:10.1093/cercor/bhq069.

Meyer H-S, Wimmer VC, Oberlaender M, de Kock CPJ, Sakmann B, Helmstaedter M. 2010. Number and laminar distribution of neurons in a thalamocortical projection column of rat vibrissal cortex. Cereb Cortex. doi:10.1093/cercor/bhq067.

Petreanu L, Mao T, Sternson SM, Svoboda K. 2009. The subcellular organization of neocortical excitatory connections. Nature. 457:1142-1145.

Pinault D. 1996. A novel single-cell staining procedure performed in vivo under electrophysiological control: morpho-functional features

of juxtacellularly labeled thalamic cells and other central neurons with biocytin or neurobiotin. J Neurosci Methods. 65:113–136.

Silver MA, Stryker MP. 1999. Synaptic density in geniculocortical afferents remains constant after monocular deprivation in the cat. J Neurosci. 19:10829–10842.

Veinante P, Jacquin MF, Deschenes M. 2000. Thalamic projections from the whisker-sensitive regions of the spinal trigeminal complex in the rat. J Comp Neurol. 420:233–243.

White EL. 1979. Thalamocortical synaptic relations: a review with emphasis on the projections of specific thalamic nuclei to the primary sensory areas of the neocortex. Brain Res. 180: 275–311.

White EL, DeAmicis RA. 1977. Afferent and efferent projections of the region in mouse SmL cortex which contains the posteromedial barrel subfield. J Comp Neurol. 175:455–482.

Wimmer VC, Nevian T, Kuner T. 2004. Targeted in vivo expression of proteins in the calyx of Held. Pflugers Arch. 449:319–333.

Woolsey TA, Van der Loos H. 1970. The structural organization of layer IV in the somatosensory region (SI) of mouse cerebral cortex. The description of a cortical field composed of discrete cytoarchitectonic units. Brain Res. 17:205–242.

Yu C, Derdikman D, Haidarliu S, Ahissar E. 2006. Parallel thalamic pathways for whisking and touch signals in the rat. PLoS Biol. 4:e124.